DOI: 10.13009/EUCASS2023-924
Aerospace Europe Conference 2023 – 10TH EUCASS – 9TH CEAS

Hybrid Rocket Engines Design for Materials Characterization

Gabriele Mangioni, Renato Marocco*, Giovanni Maria Crispino*, Daniele Bianchi**, Stefano Mungiguerra*** and Raffaele Savino****
**AVIO S.p.a, Colleferro, Italy*
gabriele.mangioni@avio.com, renato.marocco@avio.com, giovanni.crispino@avio.com
***University of Rome "La Sapienza", Rome, Italy*
daniele.bianchi@uniroma1.it
****University of Naples "Federico II", Naples, Italy*
stefano.mungiguerra@unina.it, rasavino@unina.it

Abstract

Hybrid Rocket Engines (HREs) have generated positive interest in the scientific community due to their ability to combine the special characteristics pertaining to solid and liquid propulsion [1]. Eligible as promising technology enablers for the future of space industry, HREs are valuable for their safe and controlled design nature, simplified architecture with respect to liquid engines, able to provide throttling, start/stop capabilities and in general less hazard than solid ones. One of the most profitable potentials, which is explored in this work, involves exploiting HREs as test demonstrators, particularly for materials characterization.

The aim of this work is the development of a numerical tool, whose objective is the design of lab-scale HREs for materials characterization in a specific required target application. The numerical tool is tailored on propulsion laboratory of University of Naples "Federico II" (located in military airport "F. Baracca" in Grazzanise) considering HREs ranging from 200N to 1kN thrust.

Starting from a target material application in terms of chemical environment, pressure, heat fluxes and temperature inside the combustion chamber and nozzle, the model allows to obtain a real motor configuration meeting the aforementioned constrains, analysing the following design variables: mixture ratios O/F, mass flow rates, pressures, propellant combinations, solid grain dimensions and engine scale. To complete the numerical setup and make it viable for the target material characterization, the model is paired with a routine which allows the evaluation of a suitable cost function, including several synthesis parameters that can be used globally to choose the design of the most representative lab-scale HRE. Results have been compared with CFD analyses to validate the numerical tool, especially in the evaluation of wall heat fluxes in post-chamber and nozzle throat sections and in the choice of test samples position within the rocket.

The output of this process is represented by the design of a lab-scale HRE in University of Naples "Federico II" and the production of a test matrix for specific material characterization based on suitable cost function. Thanks to its versatility, the model proposed in this work lends itself to being easily modified to study different types of materials working on different applications.

1. Introduction

The aim of the model described in this paper is the support for material thermochemical characterization that will find use and development in the space industry for several applications, such as nozzle components, thermal protections and in general space-oriented parts.
Regarding the choice of using a hybrid rocket engine to test these materials, there may be several reasons: firstly, the combustion products of a HRE contribute to generate highly oxidative environments and at highly variable concentrations depending on the configuration selected; secondly, as is well known from literature and experimental data, HREs are much cheaper than liquid rocket engines and slightly more complex than solid rocket ones in terms of applications (re-ignitable and throttleable).
The features previously introduced make this kind of application particularly suitable for nozzle extreme conditions (vacuum, aggressive oxidizing combustion products and heat fluxes).

DOI: 10.13009/EUCASS2023-924

1.1 Lab-scale HREs

The model, along with all the considerations made, is tailored on the propulsion laboratory of University of Naples "Federico II" (located in military airport "F. Baracca" in Grazzanise, CE), considering two specific configurations.

Table 1: HRE demonstrators geometric characteristics

Class	Grain			Nozzle	
	D_i [mm]	D_{max} [mm]	L [mm]	D_t [mm]	ε
200 N	15	45	70-150-220	9.6	2.99
1 kN	50	100	200-300-400	15	2.99

Concerning the two classes reported in Table 1, the 200 N motor is perfectly tested and functioning, while the 1kN class is in development phase. In the Table, D_i is the initial grain port diameter, D_{max} is the maximum allowed port diameter, L is the grain length, D_t is the nozzle throat diameter, ε is the nozzle expansion area ratio.

Before introducing the complete numerical model, a brief overview of both engines is given below.

- Axisymmetric combustion chamber
- Conical axial injector
- Upstream and downstream of the solid grain a dump plenum and an aft-mixing chamber are set up, respectively.
- A converging-diverging nozzle is employed, with a throat diameter of 9.6 mm for 200 N class and 15 mm for 1 kN class.

Figure 1 shows the layout of the 200 N engine motor.

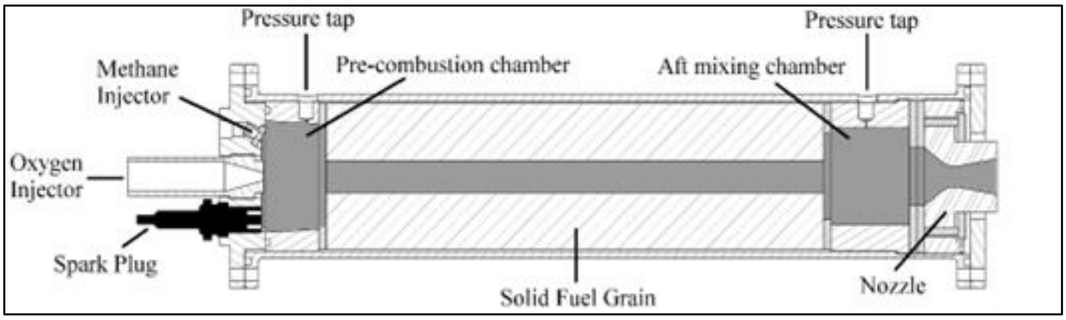

Figure 1: 200 N class engine layout

2. Numerical Model

To meet the objectives of this work, the numerical tool development follows a two-step approach:

1. a parametric analysis of the performance of hybrid propellant rockets to:
   a. identify the most interesting propellant combinations for the case to be studied.
   b. generate a set of feasible configurations depending on certain constraints imposed by the capabilities of the facility.
2. the second step, on the other hand, aims at solving an optimization process in order to select from all the configurations evaluated and collected in a database, the most representative with respect to the chosen target for material characterization purposes related to a specific application.

DOI: 10.13009/EUCASS2023-924

To ensure that the configurations studied are chemically compatible, a first quick analysis has been carried out by coupling a MATLAB routine to the NASA CEA thermochemical calculation code [2], independent of both the engine and the geometrical characteristics of the propellant grain: this process led to the isolation of a total of 3 oxidizers (namely O_2, N_2O and H_2O_2) and 3 fuel grains mixture (HTPB, HDPE and paraffin).
After choosing consistent intervals for the mixture ratio $\mathbf{O}/\mathbf{F}$, chamber pressure $\mathbf{P_c}$ and area ratio $\boldsymbol{\varepsilon}$, an improved version of the preliminary tool generates look-up tables, as many as there are combinations of propellants, containing as function of the selected constraints the following fluid properties:

- Temperature $\mathbf{T}$, pressure $\mathbf{P}$, Mach number $\mathbf{M}$, isobaric specific heat $\mathbf{c_p}$, viscosity coefficient $\boldsymbol{\mu}$, density $\boldsymbol{\rho}$, specific heat ratio $\boldsymbol{\gamma}$, molecular weight $\mathbf{m_w}$.
- Thrust coefficient $\mathbf{C_f}$, Specific impulse $\mathbf{I_{sp}}$ (used to compute the characteristic velocity $\mathbf{c}^*$).
- Chemical composition (mole fractions > 10^{-6}).

The values of such parameters are computed at three distinct stations: combustion chamber, nozzle throat and nozzle exit, assuming equilibrium condition in the convergent and frozen condition in the divergent.

2.1 Thermo-fluid dynamic database

For each combination of setup parameters, the rocket performances are evaluated through a numeric procedure, whose block diagram is provided in the following figure.

DOI: 10.13009/EUCASS2023-924

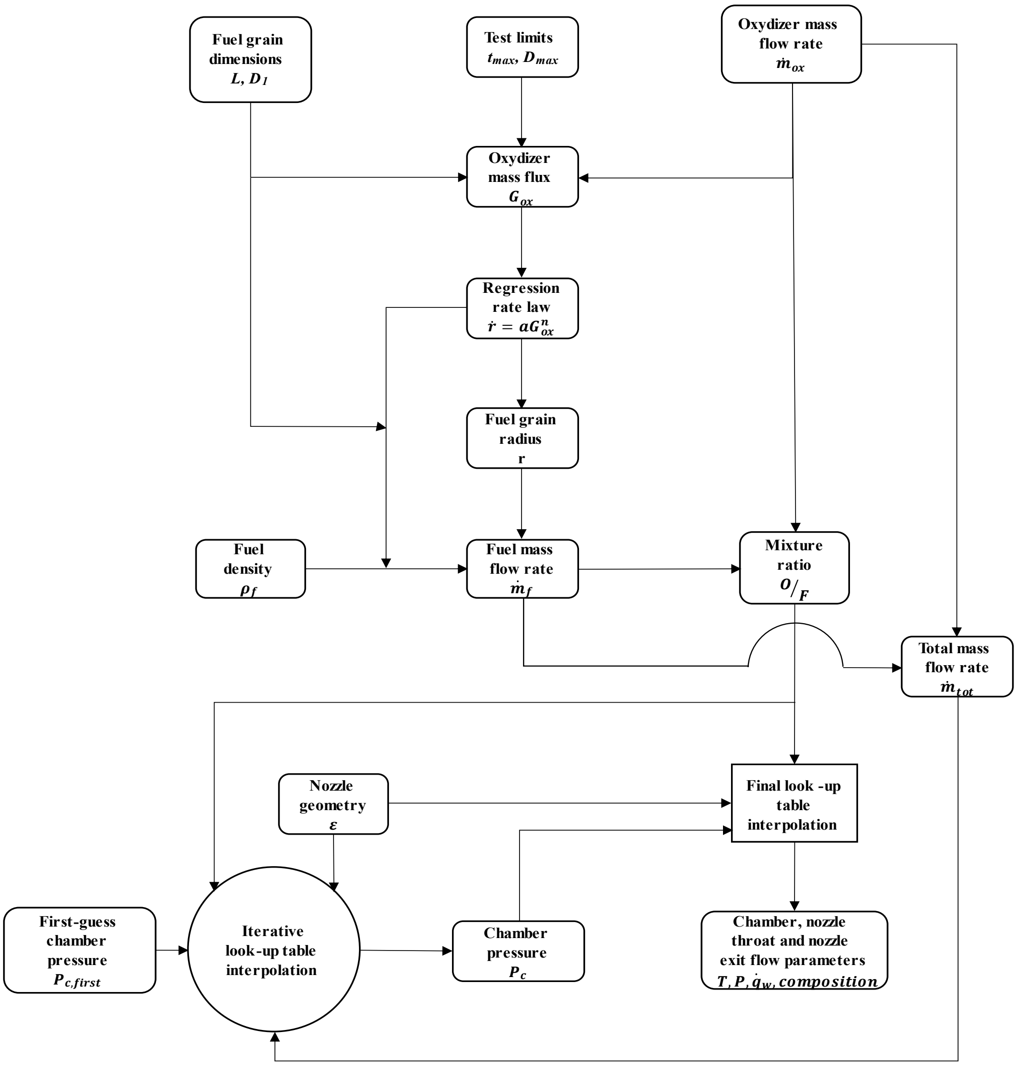

Figure 2: Thermo – fluid dynamic model flow chart

The code takes in input the fuel grain length **L**, the maximum test duration $\mathbf{t_{max}}$ and the oxidizer mass flow rate, which is the control parameter available at the facility for experimental tests.

To perform the analysis, it is needed to define the motor dimensions along with the propellant combination; there are databases for engine classes, regression rates and mixture properties: the engine file contains information about maximum diameter, chamber pressure limits and injection system features; the regression rates file contains the pre-exponential constant **a** and the exponent **n** of the chosen propellant combination regression law, whose general expression is taken from the Marxmann model [3]. This database, along with its constants, was constructed using both literature sources and post-processed experimental data.

$$\dot{\mathbf{r}} = \mathbf{a}\mathbf{G_{ox}}^{\mathbf{n}} \quad (1)$$

Finally, the mixture file contains densities of propellants at the storage temperature (299.8 K).

Starting from this input data, the code evaluates the instantaneous oxidizer mass flux $\mathbf{G_{ox}}$, which allows to compute the instantaneous regression rate $\dot{\mathbf{r}}$; subsequently, under the assumption of uniform erosion of the grain along its length, it integrates $\dot{\mathbf{r}}$ obtaining the temporal internal diameter evolution, enabling the computation of endoreactor performances.
The code calls for the previously generated look-up tables that are interpolated receiving in input the mixture ratio (already obtained), the area ratio (nozzle geometry is known) and the chamber pressure, which, however, is unknown: its value is calculated through an iterative procedure that uses the total mass flow rate as a convergence criterion.

DOI: 10.13009/EUCASS2023-924

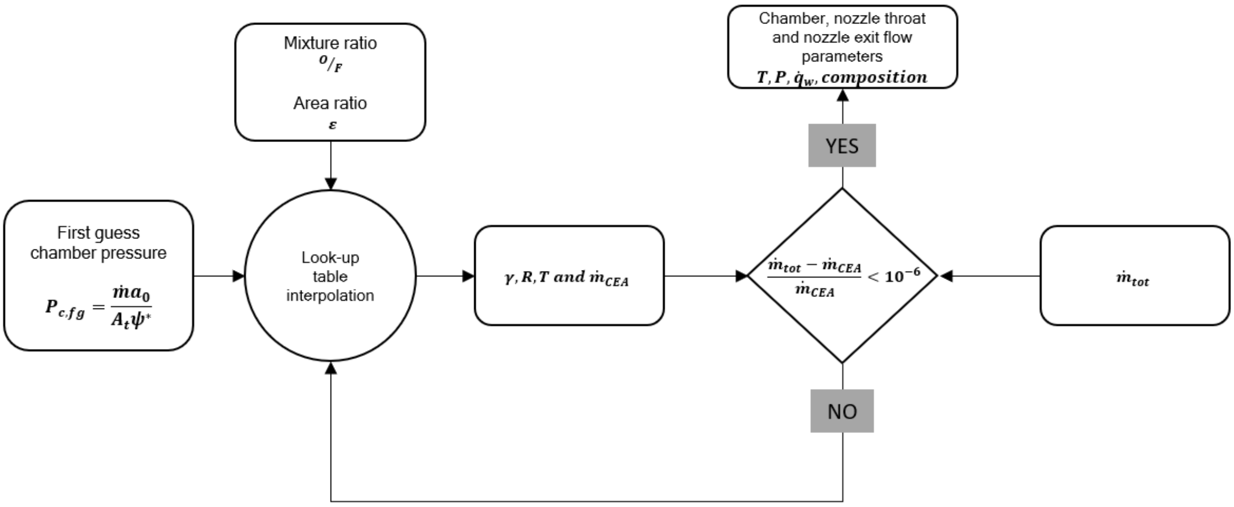

Figure 3: Thermo – fluid dynamic model convergence criterion

A root-finding algorithm (secant method) is employed to determine the real value of the chamber pressure which guarantees mass balance, namely by minimizing the following error function.

$$\mathbf{E(p_c) = \frac{\dot{m}_{tot} - \dot{m}_{CEA}}{\dot{m}_{CEA}}} \quad (2)$$

The results of the last iteration represent the real values of thermo-fluid dynamic and rocket performances.

A note worth of mention is about two important parameters that CEA itself is not natively able to compute: the test duration $\mathbf{t_{test}}$ and the wall heat flux $\mathbf{\dot{q}_w}$.

The computation of the additional parameters has been independently integrated, with particular care on the wall heat flux, obtained by coupling the code with the formula derived from Bartz theory [4], which provides the convective heat transfer coefficient $\mathbf{h_g}$**:**

$$\mathbf{h_g = \frac{0.026}{D_t^{0.2}}\left(\frac{P_c}{c^*}\right)^{0.8}\left(\frac{D_t}{D}\right)^{1.8} c_p \mu_e^{0.2}\left(\frac{T_e}{\langle T\rangle}\right)^{0.8-0.2w}} \quad (3)$$

Based on the Crocco’s analogy between total enthalpy and velocity profiles, under the assumption of flat wall, fully turbulent boundary layer and Prandtl number $\mathbf{P_r \cong 1}$. In the end, the convective heat flux is calculated in post-chamber and throat sections:

$$\mathbf{\dot{q}_w = h_g(T_{aw} - T_w)} \quad (4)$$

The wall here is assumed to be cold, so $\mathbf{T_w = 300\ K}$ and the adiabatic wall temperature is assumed to be equal to the chamber temperature $\mathbf{T_{aw} = T_c}$.

2.2 Optimization process

The optimization procedure is carried out to discriminate the most representative configuration for material characterization among all the generated ones. The parameters evaluated, along with an explanation for their choice (□[5]□[6]) within the optimization analysis have been divided in two categories: cost function parameters and engineering parameters.

DOI: 10.13009/EUCASS2023-924

Cost function parameters are used to directly build the analytical tool, whose form and characteristics are explained in the following section, and are:

1. Chemical composition: in most cases, the oxidizers are represented by water vapour (H_2O), carbon dioxide (CO_2), hydroxyl group (OH), molecular oxygen (O_2) and atomic oxygen (O): their effect can be measured in the capacity of reacting with superficial carbon and produce carbon monoxide (CO). Literature suggests that due to their poor erosion effect and/or low fractions O_2, O and OH can be neglected however it is important to stress that those species have different reaction mechanism: the reaction involving OH group is characterized by zero activation energy, so its reaction rate strongly increase with increasing temperature (at least until the kinetic control limit temperature is reached). This is the reason why, even in poor concentrations, its effect is non negligible. Atomic oxygen is both in typically low concentrations and has a very low erosive power.
   Non-oxidizing species, namely molecular hydrogen (H_2), atomic hydrogen (H) and carbon monoxide (CO), do not participate in the superficial reaction mechanisms and that's why they are not considered in this analysis. It is worth to mention that in some cases, specifically the configurations generated by using Nitrous oxide (N_2O) as propellant, there is a non-negligible amount of nitrogen (N_2, natively neutral, non-reacting), sometimes present as nitrogen dioxide (NO_2) which instead is an oxidizer: it has been neglected as well due to its poor concentration and anyway present only in few cases.

2. Test duration: one of the direct outputs of the numerical model, is a conservative estimation based on average values; it is considered a parameter of importance in defining if a configuration can be used in an endurance test scenario.

For what concerns engineering parameters, used as a filter to drive the final choice in a practical way:

a. Wall heat flux: obtained with Bartz theory, it is one of the most important synthesis parameters since it involves the dependence of other quantities, which are ablation-relevant, such as chamber pressure, mixture ratio and nozzle geometry. It is considered as one of the most important parameters also because it drives the choice of the positioning of the sample components to be tested inside the nozzle, since the gas core chemical composition slightly varies from post-chamber and nozzle throat.

b. Static temperature: the erosion process is characterized by different behaviours in dependence of the wall temperature and in literature different sources can be found that agree on defining a transition temperature under which this process is kinetic limited, driven by reaction rates temperature dependent. Above this limit there is the diffusion limited region, in which the species diffusion inside the boundary layer is slower than the kinetics. The wall temperature, obtainable by solving the surface heat balance equation, is in turn controlled by static temperature and in general stagnation temperature.

Although pressure is a key parameter, it is not explicitly considered because its effect is still present inside the wall heat flux.

The final synthesis of this work takes the form of solving an optimization problem. This strategy is justified by the fact that since we are interested in characterizing materials for specific target applications (thermo-ablative characterization) using an engine with hybrid propellants. The tool chose to proceed by sounding out all the configurations generated in the numerical analysis phase and collected in a sufficiently dense database through the definition of an optimization problem.

For this reason, the definition of an analytical tool to discriminate the best configuration among all those generated in the form of a cost function, mentioned before and now explained, is required; there are several solutions in literature, which depend mainly on the problem to be optimized and the degree of knowledge of the physical phenomena involved. The choice, after careful study, fell on the least squared method, which is a mature and well assessed criterion widely used in solving optimization problems.

The generic expression that summarizes all this work is given below.

$$\boldsymbol{Cost\ function} = \left[\sum_{j}^{N} \mathbf{w_j}\left(\mathbf{x_j^i} - \mathbf{x_j^T}\right)^2\right]^{1/2} + \boldsymbol{Engineering\ filters} \qquad (5)$$

DOI: 10.13009/EUCASS2023-924

The approach for the cost function definition is quite simple: given the target configuration for each reference engine, propellant combination, and oxidizer mass flux the difference between the cost function parameters introduced above and the corresponding targets ($\mathbf{x^i}$ and $\mathbf{x^T}$ respectively) has been evaluated, squared, and combined with proper weights that is critical for the best outcome. In addition, the counter **j** represents the number of parameters (**N**) while the counter **i** represents the motor configuration.

The parameter comparison for the cost function and engineering filters definition is given in Table *2*.

Table 2: Parameter comparison for the cost function definition

	Quantity	Importance	Comparison	Usage
Chemical composition	Variable	High	Yes	Cost function
Test duration	Variable	High	Yes	Cost function
Temperature	Extremely variable	High	Yes	Filter
Wall heat flux	Extremely variable	High	Yes	Filter

For what concerns the usage of parameters, static temperature and wall heat flux are extremely variable, negatively affecting the results of the optimization process. This behavior led to the conclusion that, to correctly navigate through the configuration space, wall heat flux should not be considered in the direct calculation of the cost function but rather used as a filter in the final choice of the optimum configuration (the same is valid also for the static temperature).

On the other hand, chemical composition and test duration are suitable for building the cost function terms.

2.3 Heat flux CFD validation

During the development of the model, it has been decided to validate the previous analysis about the wall heat flux, obtained with the Bartz formulation, with a series of CFD simulations using ANSYS Fluent.
All the efforts have been concentrated into studying a specific configuration: 200 N motor, 220 mm grain length and the H2O2-HTPB propellant combination was chosen, and the calculations have been performed on a sampled interval of oxidizer mass flow rates. The following figure is a visual representation of the mesh used for this job.

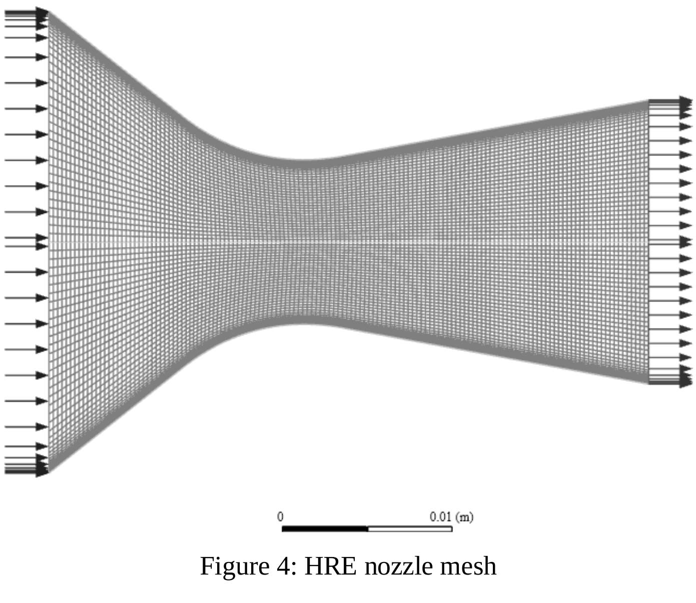

Figure 4: HRE nozzle mesh

DOI: 10.13009/EUCASS2023-924

The CFD simulations are based on a combustion process chain, modelled by 22 kinetic reactions under consideration of 12 different species: the reaction mechanism, derived from the work of Westbrook and Dryer [7], is a multistage combustion model with a quasi-global first reaction step for the reaction of 1,3-Butadiene with oxygen. A turbulent flow was considered, employing the Shear Stress Transport (SST) *k–ω* model as turbulence closure [8], and turbulence-chemistry interaction was modeled by the Eddy Dissipation Concept (EDC) model [9].

Using the described chemical reaction model, a steady-state simulation with the ANSYS Fluent solver for each oxidizer mass flow rate value was carried out, with the aim to validate the model using the convective wall heat flux.

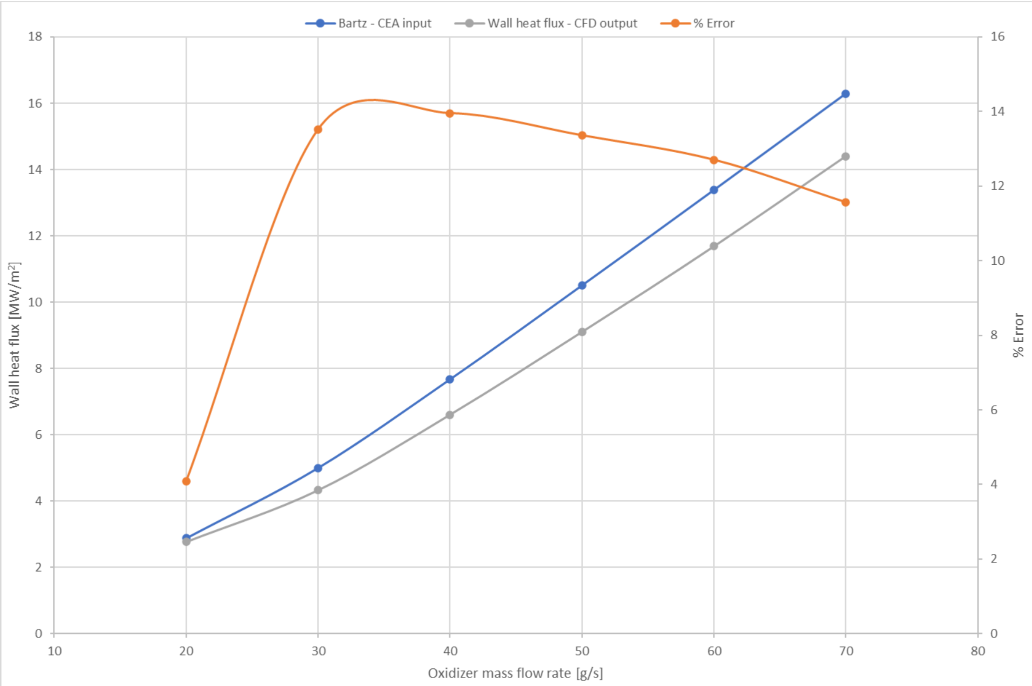

Figure 5: Wall heat flux (convective component) comparison

As it can be seen from Figure 5, there are 2 curves representing respectively the wall heat flux prediction obtained with Bartz formula and using the thermos-fluid dynamics database values (blue curve) and the heat flux values directly calculated by Fluent (gray curve).

A deviation between the curves in the range of 1 - 15 % can be appreciated.

3. Results

This tool was used to understand how best to characterize materials for a specific industrial AVIO application by discriminating an optimal test configuration: applying the algorithm outlined in numerical model section to the fixed oxidizer mass flow rate intervals produced a total of 7272 configurations, of which 1836 belongs to the small-scale engine and 5436 to the large-scale one.
Given the engine configuration, the procedure introduced in the previous section has been applied to all propellant combinations (H2O2, O2 and N2O as oxidizers, HTPB and HDPE as fuels) and for $\dot{\mathbf{m}}_{\mathbf{ox}}$ varying from 20 to 70 g/s for the small scale and from 100 to 250 g/s for the large one.

3.1 Optimum configuration discrimination

As described in the previous chapter, the cost function named **J** has been evaluated using the following variables, where $_T$ represents the Target of the specific application, while $_i$ represents the i-th motor configuration.

$$\mathbf{J} = \sqrt{\mathbf{w_{H2O}}([\mathbf{H_2O}]_i - [\mathbf{H_2O}]_\mathbf{T})^2 + \mathbf{w_{CO2}}([\mathbf{CO_2}]_i - [\mathbf{CO_2}]_\mathbf{T})^2 + \mathbf{w_{time}}(\mathbf{t}_i - \mathbf{t_{lim}})^2} \qquad (6)$$

DOI: 10.13009/EUCASS2023-924

Following the logic of the optimization procedure, the configuration characterized by the minimum cost function is the analytical optimum. However, this solution does not necessarily close the problem: the cost function does not embed everything and needs a further engineering critical analysis.
As can be seen in Table 2, apart from the variables that contribute directly to constructing the cost function, there is a "filter" tag assigned to temperature and wall heat flux that will be used in the final choice. The idea is always to give priority to the cost function but choosing the most feasible solution in engineering terms.

In the following graph, it is possible to appreciate the value of the 3 minimum cost functions relative to 3 different motor configurations, each of which is associated with a textbox containing the main information useful for the potential execution of a preliminary test. A polar diagram has been considered the proper way to show the best configurations, since the distance of the points from the center (target) is precisely the value of J. Finally, it is possible to note the presence of other scattered points, in light grey, representative of the other configurations that were discarded for this specific case study (precisely 7269). The three highlighted configurations are the best in terms of cost function and the same convention on symbols is adopted for all the figures in this paragraph.

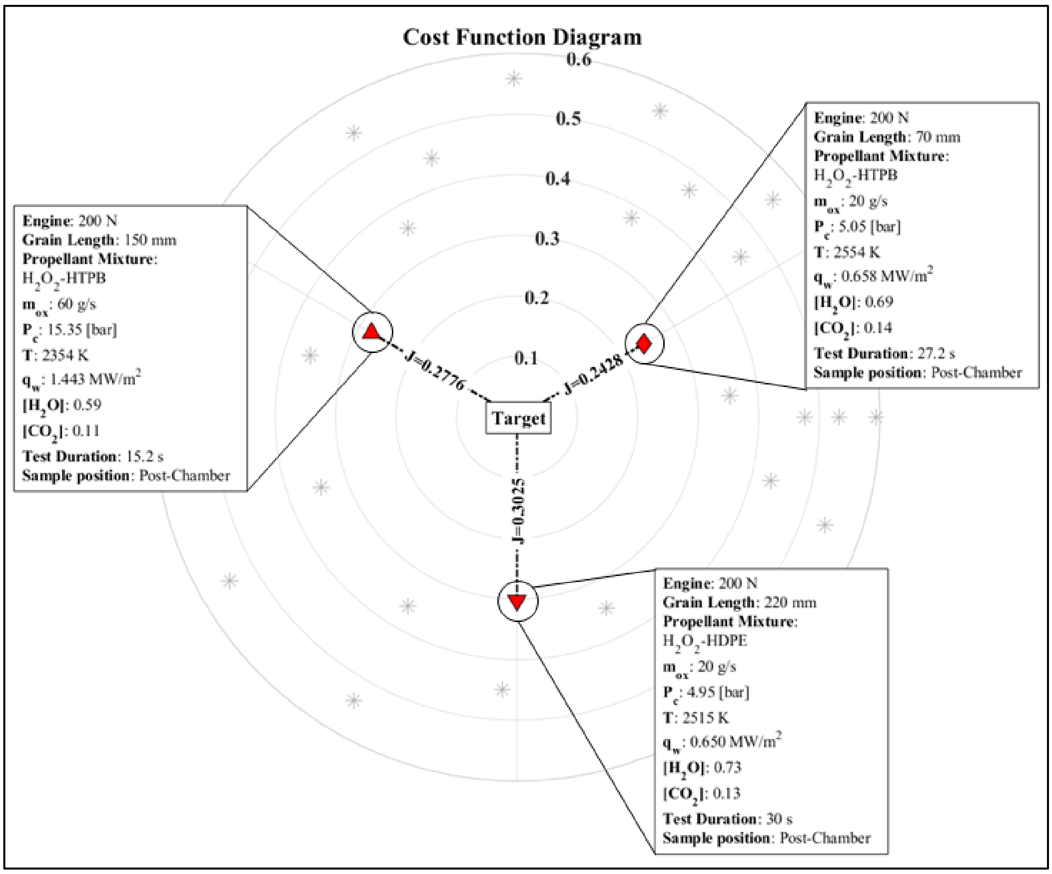

Figure 6: Cost function diagram

The following table represents the core of this work, where the ultimate results are shown.

DOI: 10.13009/EUCASS2023-924

Table 3: Optimization process results

Symbol	◆	▲	▼
Cost Function J	0.2428	0.2776	0.3025
Engine	200 N	200 N	200 N
Grain length, [mm]	70	150	220
Propellant mixture	H2O2-HTPB	H2O2-HTPB	H2O2-HDPE
$\dot{m}_{ox}$, [g/s]	20	60	20
T , [K]	2554	2354	2515
P_c , [bar]	5.05	15.35	4.95
$\dot{q}_w$, [MW/m2]	0.658	1443	0.650
$[H_2O]$	0.69	0.59	0.73
$[CO_2]$	0.14	0.11	0.13
Test time, [s]	27.2	15.2	30

The following graph shows all the configurations generated in a scatter plot, distinguished according to the engine in which they were obtained and in dependance of Static Temperature and Wall heat flux.

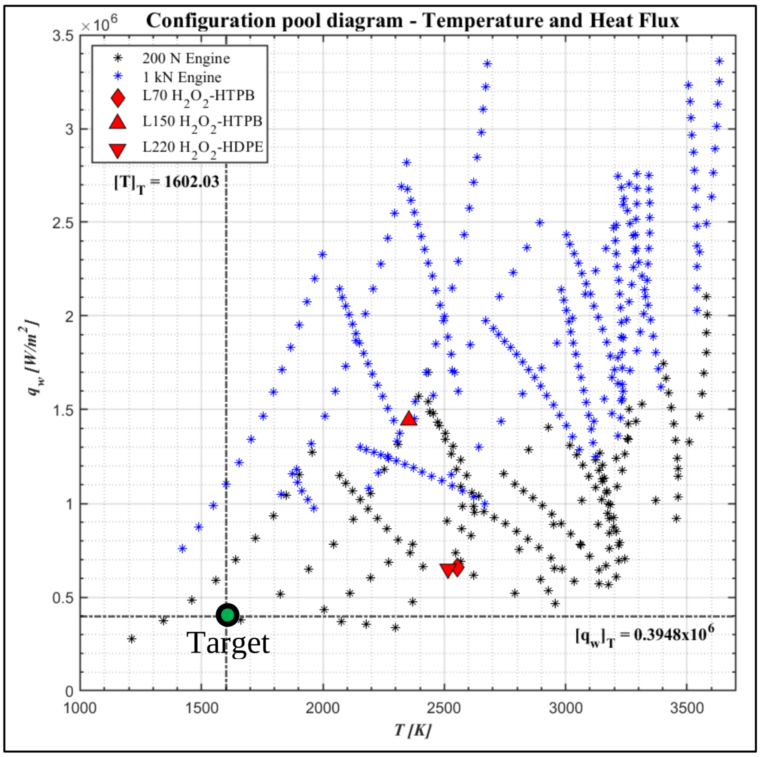

Figure 7: Post-chamber section configuration pool as a function of temperature and wall heat flux

It is worth to mention that many configurations have been excluded from the figure as they pertain to the throat section: as mentioned several times, the heat flux in the throat is too high for this specific analysis, so the model, despite being able to process these configurations, excludes them. From now on, every case shall be automatically considered evaluated in the post-chamber section of the nozzle.

DOI: 10.13009/EUCASS2023-924

Another interesting figure is the following, which represents the same pool of configurations but in terms of test duration.

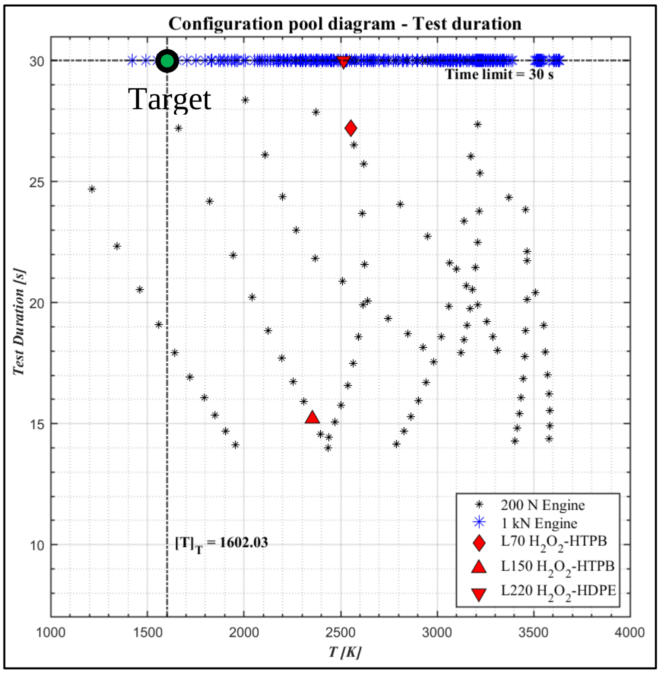

Figure 8: Post-chamber section configuration pool as a function of temperature and test duration

As it can be seen, every point belonging to 1 kN class engine lies on the 30 s limit (imposed on the facility capabilities): this is due to bigger dimensions of the grain, while the smaller class is characterized by uniformly distributed times between 14 and 30 s, depending on both grain length and oxidizer mass flow rate: the higher the mass flow rate, the lower the execution time.

3.2 Engineering analysis

The choice of the best configuration for the case of study is better understood if paired with the following figures.

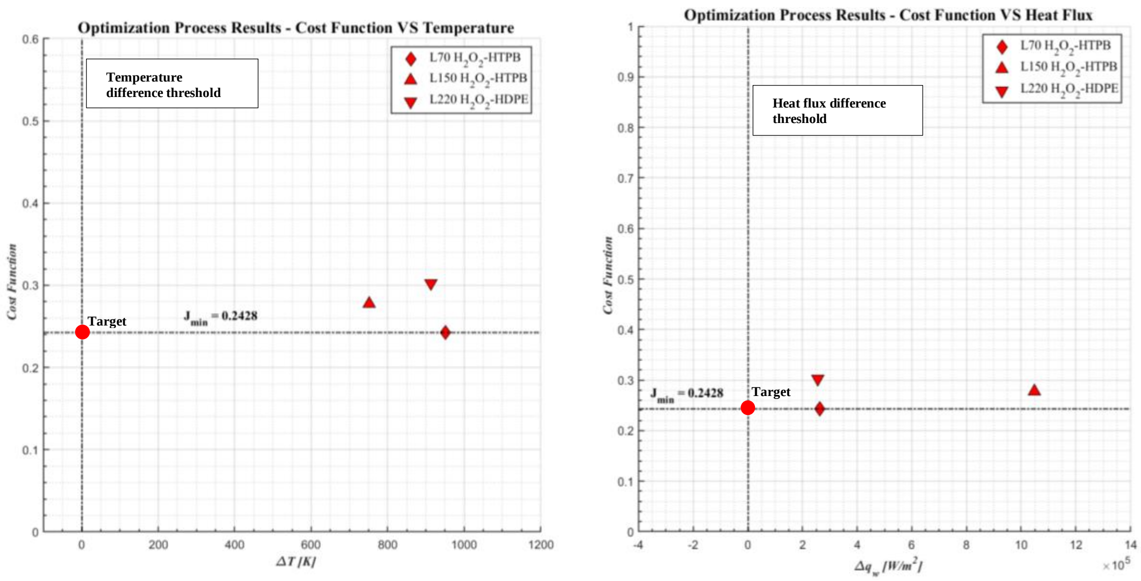

a) Cost function VS Temperature

b) Cost function VS Wall heat flux

Figure 9: Final choice discrimination

DOI: 10.13009/EUCASS2023-924

Both graphs represent the same 3 configurations as a function of the cost function value and the differences in a) Temperature and b) Heat Flux respectively; there are also represented two dotted lines, again one for the difference with respect to the target and the other for the minimum cost function threshold: this limit is imposed by the diamond-shaped symbol, which finally is the configuration chosen by the algorithm. Then there is the upward-facing triangle, which has the lowest temperature difference, and the downward-facing triangle, with the lowest heat flux difference.

In this case the engineering choice falls on the diamond one because its heat flux is comparable and the difference in temperature does not differ too much with respect the target.

4. Conclusions

A numerical tool to support the thermo-ablative characterization of materials used in the space industry and the design of demonstrators for test campaigns was developed. It was decided to support this tool by fusing it with a purely engineering data analysis, to avoid solutions that are numerically correct but not physically and practically compatible. The model presented in this work was validated on wall heat fluxes (convective component) by means of CFD analysis for a single case, to demonstrate the goodness of the results obtained. Finally, the tool was applied for a specific industrial target of AVIO. The result of the analysis performed will then be used to design and develop a specific motor demonstrator and perform tests on the selected materials accordingly.

References

[1] Mungiguerra S., Di Martino G. D., Savino R., Zoli L., Silvestroni L., Sciti D., Characterization of novel ceramic composites for rocket nozzles in high-temperature harsh environments, International Journal of Heat and Mass Transfer 163 (2020)

[2] S. Gordon and B. J. McBride, "Computer Program for Calculation of Complex Chemical Equilibrium Compositions and Applications," NASA Reference Publication 1311 (1996).

[3] Zilliac G., Karabeyoglu M. A., Hybrid rocket fuel regression rate data and modelling, in 42nd AIAA/SAE/ASEE Joint Propulsion Conference & Exhibit, Sacramento, California, 2006, AIAA.

[4] Bartz, D. R., Turbulent boundary-layer heat transfer from rapidly accelerating flow of rocket combustion gases and of heated air, Advances in Heat Transfer, Vol. 2, 1965, 1-108

[5] Bianchi, D.,Nasuti, Numerical analysis of nozzle material thermochemical erosion in hybrid rocket engines, F.Journal of Propulsion and Power, 2013, 29(3), pp. 547–558.

[6] S. T. KESWANI, K. K. KUO, Validation of an Aerothermochemical Model for Graphite Nozzle Recession and Heat-Transfer Processes, Combustion Science and Technology, 47:3-4, 177-192.

[7] Westbrook, C. K., and F. L. Dryer. 1981. Simplified Reaction Mechanisms for the Oxidation of Hydrocarbon Fuels in Flames. Combustion Science and Technology. Vol. 27, pp. 31-43.

[8] Menter, F.R., Two-Equation Eddy-Viscosity Turbulence Models for Engineering Applications, *AIAA Journal*, Vol. 32, No. 8, 1994, pp. 1598-1605

[9] Magnussen, B.F., On the Structure of Turbulence and a Generalized Eddy Dissipation Concept for Chemical Reaction in Turbulent Flow, In: *Nineteenth AIAA Meeting*, St. Louis, 1981.